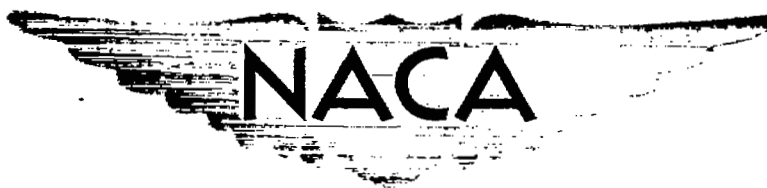


NACA RM No. L9C11



RESEARCH MEMORANDUM

STUDY BY NACA WING-FLOW METHOD OF TRANSONIC DRAG
CHARACTERISTICS OF A BLUNT-NOSE BODY OF
REVOLUTION AND COMPARISON WITH RESULTS
FOR A SHARP-NOSE BODY

By

J. Ford Johnston and Mitchell Lopatoff

Langley Aeronautical Laboratory
Langley Air Force Base, Va.

CLASSIFICATION CANCELLED

CLASSIFIED DOCUMENT

Authority *NACA R7 2423*

Date *8/19/54*

By *J.F.J. 9/24/54*

See

This document contains classified information affecting the National Defense of the United States within the meaning of the Espionage Act, USC 31 and 32. Its transmission or the revelation of its contents in any manner to an unauthorized person is prohibited by law. Information so classified may be imparted only to persons in the military and naval services of the United States, appropriate civilian officers and employees of the Federal Government who have a legitimate interest therein, and to United States citizens of known loyalty and discretion who of necessity must be informed thereof.

NATIONAL ADVISORY COMMITTEE FOR AERONAUTICS

WASHINGTON

April 26, 1949



UNCLASSIFIED

NATIONAL ADVISORY COMMITTEE FOR AERONAUTICS

RESEARCH MEMORANDUM

STUDY BY NACA WING-FLOW METHOD OF TRANSONIC DRAG

CHARACTERISTICS OF A BLUNT-NOSE BODY OF

REVOLUTION AND COMPARISON WITH RESULTS

FOR A SHARP-NOSE BODY

By J. Ford Johnston and Mitchell Lopatoff

SUMMARY

A body of revolution with an NACA 1-50-100 nose inlet at zero angle of attack and no internal air flow was selected for study by the NACA wing-flow method of the pressure drag of an extremely blunt-nose body and comparison with previous results for a sharp-nose body.

For the body with nose inlet, local sonic velocity was first attained at the inlet lip at Mach number $M = 0.76$ and at the maximum thickness position at $M = 0.83$, but the drag rise did not begin until $M = 0.90$. The pressure drag coefficient rose from zero at $M = 0.90$ to 0.25 at $M = 0.98$ and to 0.38 at $M = 1.10$.

The change from sharp to inlet nose while maintaining the same after-body shape decreased the drag-rise Mach number from 0.94 to 0.90.

The general nature of the pressure-drag variation with Mach number for slender bodies of revolution in the transonic range is tentatively proposed from consideration of the separate drag contributions of front and rear ends.

UNCLASSIFIED

INTRODUCTION

The drag characteristics of sharp-nose bodies of revolution have been investigated by the NACA wing-flow method (reference 1) and free-fall method (reference 2) in the transonic speed range. Results from the free-fall investigations indicated that the body shape behind maximum thickness was the controlling factor in the drag rise below Mach number 1.0. From the wing-flow tests it was concluded that the drag rise below Mach number 1.0 was due principally to the growth and rearward shift of the peak negative pressure beyond the maximum thickness position. The drag rise of the wing-flow model occurred shortly after the local velocity of sound was attained at maximum thickness on the body. Additional drag increases above Mach number 1.0 appeared in both investigations to be governed primarily by the portion of the body in front of the maximum thickness position.

In order to investigate further the effect of forebody shape at transonic speeds, an extreme case of a nose inlet at zero inlet-velocity ratio and zero angle of attack was selected for study of the pressure drag by the wing-flow method. The afterbody selected was the same as that of the sharp-nose body tested by the same method (reference 1). The inlet shape was one already tested (with a different afterbody) up to Mach number 0.92 in the Langley 8-foot-high-speed tunnel (reference 3). The results of the investigation are reported herein.

APPARATUS AND METHOD

A sketch of the model used showing dimensions, inlet proportions, and orifice locations is shown in figure 1, and a photograph of the model is given as figure 2. The portion of the model ahead of maximum thickness was very closely an NACA 1-50-100 nose inlet; that is, an inlet having the NACA series 1 external ordinates given in reference 4, with inlet diameter 50 percent of the maximum diameter and the length equal to the maximum diameter. The inlet duct was blanked off one inlet diameter behind the nose. The portion of the model behind maximum thickness was of circular-arc profile and was supported on a half-inch diameter sting; these rear-section ordinates and the sting size were the same as for the sharp-nose body of reference 1. The upper and lower meridian lines each carried 12 static-pressure orifices spaced along the body as shown in figure 1. A single orifice was also placed in the center of the inlet for measurement of the internal pressure recovery. The upper- and lower-surface orifices at a given position x/D were tied into a single pressure line at the center of the body. By this means the average of the upper- and lower-surface pressures was measured directly for each x/D . As in reference 1, the average pressure was assumed to represent the pressure at zero angle of attack. The

body-sting combination was mounted 6 inches above the airplane wing as shown in figure 3 and was aligned laterally with the local flow.

Mach number at the model position was obtained by the use of two pressure tubes located 8 inches on each side of the model with two static orifices on each tube as shown in figure 4. The average of the Mach numbers from these four positions was used as the Mach number at the model position. It was determined that the presence of the model did not appreciably affect the average. The normal and longitudinal Mach number gradients at the test section are described in reference 1. It was concluded in reference 1 that the longitudinal gradients were small with respect to those on the model and should have small effect on the position of separation. It has been found in practice that the pressure drag should not be corrected for horizontal buoyancy due to the longitudinal gradients existing without the model in place.

The experimental technique was to dive the aircraft from an altitude of 28,000 feet at a Mach number of 0.50 to 15,000 feet and a Mach number of 0.71 which gave corresponding local Mach numbers of 0.70 to 1.10, respectively. Eight 12-second records were also obtained at constant Mach numbers to supplement data recorded in the dive. During these runs, standard NACA instruments continuously recorded and synchronized all model pressures and supplementary information such as airplane impact and static pressures.

RESULTS AND DISCUSSION

Variation of pressure coefficient with Mach number.— The basic data are presented in figure 5 as the variation of pressure coefficient $\Delta p/q$ (local pressure above stream static as fraction of the dynamic pressure q) with Mach number M for each orifice position x/D . On the portion of the body in front of maximum thickness (figs. 5(a) to 5(f)) the variation of pressure coefficient with Mach number is large but fairly smooth. These forward positions are characterized by the attainment of peak negative pressure coefficients at Mach numbers in the range 0.70 to 0.95, followed by smooth but fairly rapid changes toward positive pressures. Behind maximum thickness, however, (figs. 5(g) to 5(l)) the changes in pressure are large and abrupt between $M = 0.85$ and $M = 1.00$. These large abrupt changes indicate a rapid growth and rearward shift of the negative pressures in this Mach number range.

Pressure distribution along the body axis.— The pressure distributions along the body axis at selected Mach numbers from 0.70 to 1.10 are shown in figure 6. Also shown are pressure distributions measured on a similar NACA 1-50-100 nose inlet (with a cylindrical center section between nose and afterbody, also sketched in fig. 6) at zero inlet-velocity ratio in the Langley 8-foot high-speed tunnel (reference 3)

up to $M = 0.92$, as well as the distributions on the same rear-end shape from tests of the sharp-nose body (reference 1).

It may be seen that the distributions on the tunnel and wing-flow inlet sections have the same general shape at Mach numbers of 0.70 to 0.80, but the negative pressure peak at the lip of the tunnel model is not so high and tends to disappear at lower Mach number than for the wing-flow model. The difference is probably associated with the lower mutual interference between the forebody and afterbody of the tunnel model. The effect of this interference will be discussed later.

For the wing-flow model, local sonic velocity is first attained at the lip at Mach number $M = 0.76$ and at the maximum thickness position at $M = 0.83$. The velocities over the entire inlet section up to maximum thickness are supersonic at Mach number 0.85.

The difference in rear-end pressure distributions between the models with blunt and sharp front ends indicates the extent to which the velocities induced by the inlet carry over to the rear section. This interference leads to the earlier attainment of supersonic velocities on the rear end. The formation of a pronounced shock at maximum thickness at Mach number 0.90 and its rapid rearward movement with increasing Mach number is also indicated in figure 6. The positive pressures at the last orifice indicate that there is no appreciable flow separation at the rear of the body; hence, the drag rise is associated with the primary flow rather than with any boundary-layer shock interaction. It was demonstrated in reference 1 that separation did not occur on the sharp-nose body with stings of one-half and one-fourth the body diameter. Therefore, these results should be applicable at full-scale with body-jet-diameter ratios of the same order.

Pressure drag.— Sample curves of $\Delta p/q$ plotted against the frontal area ratio $(r/R)^2$ are shown in figure 7. The area enclosed by such a curve is, with proper regard to sign, equal to the pressure drag coefficient C_D of the body-sting combination, based on frontal area. Similarly, the drag contributions of the front and rear portions of the body may be obtained by integrating the area between the x-axis and the portions of the curve representing the front and rear ends, respectively. It will be noted that the curves are closed by the stagnation pressure acting within the inlet and stream static pressure over the cross section of the sting. In this respect the sting may be assumed to represent a parallel jet of the same diameter.

The pressure drag coefficients plotted against Mach number for the inlet body are given in figure 8, along with a breakdown of the drag contributions of the front and rear parts of the body and a comparison with the drags measured on a similar inlet in the Langley 8-foot high-speed tunnel (reference 3 and unpublished data). The pressure drag coefficient for the entire body (fig. 8) increased rapidly from about

zero at $M = 0.90$ to 0.26 at $M = 0.98$ to 1.00. This abrupt increase in drag at $M = 0.90$ is associated with the formation of a supersonic region behind maximum thickness. It is to be noted in particular that the existence of an extensive supersonic region on the forward portion of the body below $M = 0.90$ did not cause an increase in the drag. Above $M = 1.00$ the drag increased again, but not as sharply, reaching 0.38 at $M = 1.10$. The total body drag curve, including skin friction, from the tunnel tests of the NACA 1-50-100 inlet with an afterbody of somewhat higher fineness ratio, as described in reference 3, shows a slight drag rise between $M = 0.85$ and $M = 0.90$, followed by a steep drag rise above $M = 0.90$. The wing-flow and tunnel results are considered to be in reasonable agreement, although the longer afterbody would be expected to give slightly high drag-rise Mach number.

The origins of the body drag may be evaluated by reference to the front- and rear-end drags also given in figure 8. It should be noted that the component drags are not generally independent of each other, inasmuch as the drag of one part is influenced to some extent by the induced velocities from the other part of the body. The exception is the nose portion above Mach number 1.0. The effect of mutual interference on the component drag below the drag-rise Mach number is the difference of each component drag from zero, inasmuch as without interference or separation potential flow requires that the pressure drag of both be zero. In this connection it is interesting to note that the pressure drag of the forebody is negative at the lower speeds because of the mutual interference. Since the forebody-afterbody mutual interference of the tunnel model was negligible, the forebody drag must be zero, and therefore the pressures on the inlet section must be generally less negative than those on the same section of the wing-flow model, as indeed they have been shown to be (fig. 6).

It may be seen that the drag rises for both parts of the body begin at $M = 0.90$, but the rate of rise for the rear end below $M = 0.98$ is considerably higher than for the front end. At $M = 0.98$, the rear-end drag is about 75 percent of the total drag. Above this Mach number, the rear-end drag coefficient drops slightly and then levels off, becoming only 45 percent of the total drag at $M = 1.10$, the extent of these tests. The test point from the Langley 8-foot high-speed tunnel at $M = 1.2$ indicates that the inlet pressure drag continues to rise at about constant rate at least to that Mach number.

A similar drag breakdown of the sharp-nose body of reference 1 into the component front- and rear-end drags is given in figure 9. Here it may be seen that the drag rise of each component begins at about $M = 0.94$. The rear end contributes about 87 percent of the total drag at $M = 0.98$ and about 66 percent at $M = 1.075$. The curves are generally similar to those of the nose-inlet body (fig. 8).

These curves are repeated in figure 10 to give a direct comparison of the total and component drags of the nose-inlet and sharp-nose bodies. It is seen that the change from sharp to inlet nose decreased the drag-rise Mach number from 0.94 to 0.90. Inasmuch as the drag rise did not begin upon the formation of supersonic velocities on the nose section, it is indicated that the drag rise is associated with the development of an appreciable supersonic region behind the maximum thickness position. The effect of the blunter nose was apparently to increase the induced velocities behind maximum thickness and thus to encourage the earlier development of supersonic velocities there. The fact that the front-end drag rise occurs for each body at the same time as the rear-end drag rise is probably an indication of the decay of the mutual interference between the front and rear ends which at subcritical speeds kept the net drag zero.

The drag rise accompanying the extensive supersonic field may be interpreted as the result of shock loss, or of pressure drag due to excessive negative pressures on rearward-sloping surfaces, or of breakdown of "signals" between front and rear of the body. All these views are correct in this case. In terms of shock loss, it may be assumed that recompression from supersonic velocities is accomplished nearly isentropically until the extent of the supersonic region becomes large along and, therefore, also away from the body. In terms of signals, it is apparent that a compression signal from the rear can go around a supersonic region if that region extends only a small distance from the surface. In so doing, part of the compression signal will compress the supersonic field at right angles to the velocity and, therefore, without shock. In these terms, then, the drag rise is not expected to become appreciable until an "extensive" supersonic field is formed. The view of the excessive negative pressures accompanying the supersonic field is narrower, inasmuch as it does not consider the whole body. In particular it may be noted that an extensive supersonic field was formed on the cylindrical section (that is, behind the first position of maximum thickness) of the tunnel model of reference 3 coincident with the drag rise. The associated negative pressures could not produce drag, inasmuch as the surface slope in this region was zero. The pressures on the after-body were unaffected, but the nose pressures became more positive. Thus, in the case of reference 3, it may be said that the shock losses became appreciable when the supersonic region moved downstream of the first position of maximum thickness, the movement onto the straight portion indicating a large vertical extent of the field; the shock losses must appear as pressure drag and take the form here of more positive pressures on the nose due to failure of expansion signals from downstream.

From the foregoing considerations, it may be concluded that the early supersonic region at the inlet lip was of such small extent away from the body as not to cause a measurable drag increase. The small lateral extent of the supersonic region is a direct result of the high

profile curvature at the lip, inasmuch as the decrease of the induced velocities with distance from the surface is proportional to the profile curvature.

The inlet body shows higher drag than the sharp-nose body at all Mach numbers above 0.90. Below $M = 0.99$, both front and rear portions contribute to the higher drag, but at higher Mach numbers the two rear-end drags are substantially the same and the increased total drag is due solely to the blunter inlet portions. The high drag cost of the blunt front end with increasing supersonic speeds is illustrated in both figures 8 and 10. It should be emphasized here that the "inlet" section should not be considered as an operative nose inlet but merely an extreme case of a blunt-nose body, which might occur if aerodynamic characteristics were completely sacrificed in favor of some other required function. The similarity to an operative nose inlet occurs in the case of a power-off dive, where high drag is usually desirable except when due to sudden power-plant failure.

If, in general, the front-end drag continues to rise until attachment of the bow shock wave, then the nose-inlet drag will probably continue indefinitely to rise with Mach number for all constant inlet-velocity ratios below 1.0. For the sharp-nose body, the bow wave theoretically attaches at $M = 1.15$, which is beyond the limit of these tests. The front- and rear-end drag coefficients have been calculated for this Mach number by the linearized theory (reference 5) and are also plotted in figure 10. It may be seen that the calculated values for the component drags are in reasonable agreement with the values obtained by extrapolation of the experimental curves to the shock-attachment Mach number. The agreement indicates that the linearized theory becomes applicable for first-order drag determination at the Mach number for attachment of the bow shock wave. Above this Mach number, the drag coefficient is expected to remain constant or to decrease slightly in accord with the theory. It will be noted that the free-fall test body of fineness ratio 12 (reference 2), having a shock-attachment Mach number of 1.05, showed peak drag coefficient at $M = 1.05$ and a slight decrease with further increase in Mach number.

On the basis of this evidence, a general picture of the pressure-drag variation for slender bodies of revolution between the subsonic force-break Mach number and the supersonic shock-attachment Mach number may be proposed tentatively from consideration of the front- and rear-end drag contributions:

1. The drag rises for the front and rear ends will begin at the same Mach number unless these components are so separated by a cylindrical center section as to make their mutual interference negligible.
2. The front-end drag coefficient varies approximately linearly between the force-break and shock-attachment Mach numbers. The lower

value of the drag coefficient can be obtained from subsonic theory or wind-tunnel tests and the upper value from supersonic theory or supersonic wind-tunnel tests.

3. The rear-end drag coefficient reaches a maximum at Mach number very near 1.0, then decreases slightly (apparently 10 percent to 20 percent) up to the shock-attachment Mach number. Again, the values at either end can be determined from subsonic and supersonic theory or experiment. It appears from figure 10 that peak rear-end drag-coefficient values are reached at $M = 1.00$ to 0.98 , depending upon the strength of the velocities induced by the front end.

A major factor in use of these deductions is determination of the force-break Mach number. High-speed subsonic wind tunnels should be satisfactory for this purpose if the choking Mach number is sufficiently higher than the force-break Mach number. If these facilities are unavailable, it is necessary to resort to predictions based on low-speed tests or theoretical pressure distributions. The predictions are uncertain not only because of the uncertainty of extrapolating the pressures to high Mach number but also because of difficulty in setting criteria for the force-break Mach number based on these extrapolated pressures.

It is already established that the occurrence of sonic velocity either at the highest speed point on the body or at maximum thickness is not a sufficient criterion for determining the force-break Mach number. It appears that the drag rise does not become appreciable until a fairly extensive supersonic field is established downstream of maximum thickness. Possibly, a general relationship exists between the critical and force-break Mach numbers. For example, it was found that for the two bodies tested, the force-break Mach number could be approximated by the formula:

$$M_{FB} = M' + \frac{1}{3}(1.0 - M')$$

where

M_{FB} stream Mach number for beginning of steep drag rise

M' stream Mach number for occurrence of local sonic velocity at maximum thickness position

This formula cannot be considered general inasmuch as only two bodies having the same afterbodies are considered. It appears that further studies should be made to predict the force-break Mach number.

CONCLUSIONS

Pressure distributions over a body of revolution with a nose inlet (with no inlet air flow) obtained at transonic speed by the NACA wing-flow method have indicated that:

1. Although local sonic velocity was first attained at the inlet lip at Mach number $M = 0.76$ and at the maximum thickness position at $M = 0.83$, the drag rise did not begin until $M = 0.90$.
2. The pressure drag coefficient rose from zero at $M = 0.90$ to 0.26 at $M = 0.98$ and to 0.38 at $M = 1.10$.
3. The drag coefficient of the portion of the body behind the maximum-thickness position reached a maximum at $M = 0.98$, then dropped slightly at higher Mach numbers. This rear-end drag was about 75 percent of the total drag at $M = 0.98$ and only 45 percent of the total at $M = 1.10$.
4. The drag coefficient of the portion of the body ahead of the maximum thickness position increased linearly with Mach number between $M = 0.90$ and $M = 1.10$, the limit of the tests.

Comparison of the results for the body with nose inlet with results for a sharp-nose body having the same rear end indicates that:

5. The change from sharp to inlet nose decreased the drag-rise Mach number from 0.94 to 0.90, presumably because the blunter nose increased the induced velocities over the rear end.
6. The general nature of the pressure-drag variation with Mach number for slender bodies of revolution in the transonic range may be proposed tentatively from consideration of the separate drag contributions of the front and rear ends:

(a) The drag rises for both components usually begin at the same Mach number because of the mutual interference existing between forebody and afterbody.

(b) The front-end pressure drag coefficient varies approximately linearly between the values at the subsonic force-break and the supersonic bow-wave-attachment Mach numbers. The lower value can be obtained from subsonic theory or wind-tunnel tests and the upper value, from supersonic theory or wind-tunnel tests.

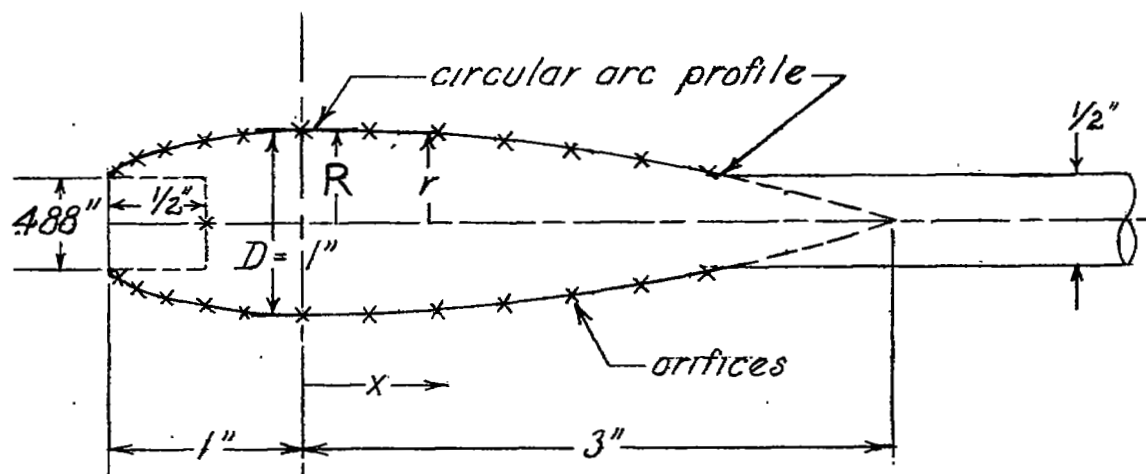
(c) The rear-end pressure drag coefficient reaches a maximum at Mach number very near 1.0, then decreases slightly up to the bow-wave-attachment Mach number. Again, the values at either end can be determined from subsonic or supersonic theory or experiment.

(d) The linearized supersonic theory becomes applicable for determination of the body pressure drag at the Mach number for bow-wave attachment.

Langley Aeronautical Laboratory
National Advisory Committee for Aeronautics
Langley Air Force Base, Va.

REFERENCES

1. Danforth, Edward C. B., and Johnston, J. Ford: Pressure Distribution over a Sharp-Nose Body of Revolution at Transonic Speeds by the NACA Wing-Flow Method. NACA RM No. L7K12, 1948.
2. Thompson, Jim Rogers, and Kurbjun, Max C.: Drag Measurements at Transonic Speeds of Two Bodies of Fineness Ratio 9 with Different Locations of Maximum Body Diameter. NACA RM No. L8A28b, 1948.
3. Pendley, Robert E., and Smith, Norman F.: An Investigation of the Characteristics of Three NACA 1-Series Nose Inlets at Subcritical and Supercritical Mach Numbers. NACA RM No. L8L06, 1949.
4. Baals, Donald D., Smith, Norman F., and Wright, John B.: The Development and Application of High-Critical-Speed Nose Inlets. NACA ACR No. L5F30a, 1945.
5. Jones, Robert T., and Margolis, Kenneth: Flow over a Slender Body of Revolution at Supersonic Velocities. NACA TN No. 1081, 1946.

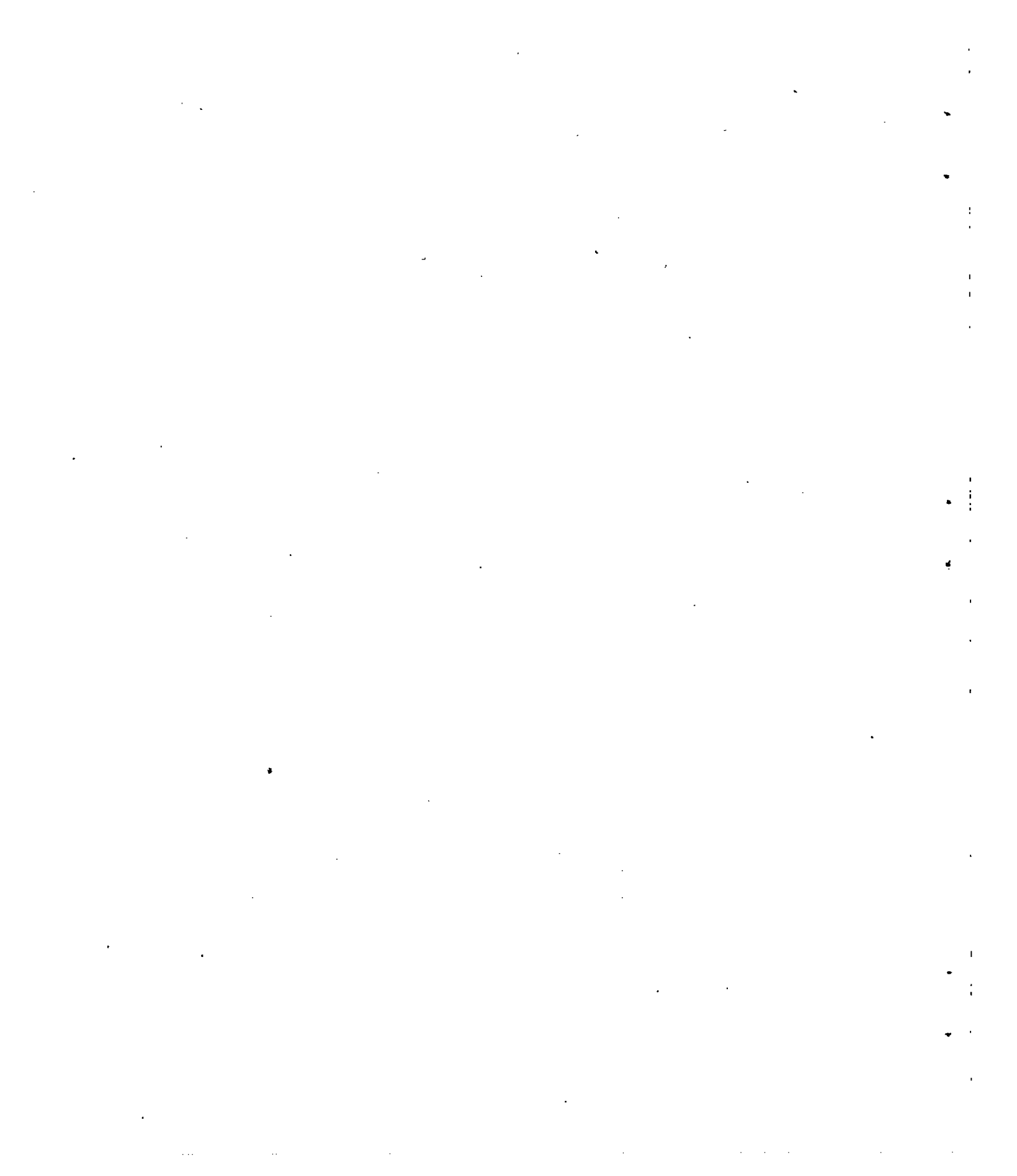


Orifice locations for upper and lower meridian

Front		Rear	
$\frac{x}{D}$	$\frac{r}{R}$	$\frac{x}{D}$	$\frac{r}{R}$
-.975	.575	.360	.979
-.850	.728	.710	.958
-.700	.815	1.070	.934
-.500	.898	1.400	.869
-.300	.955	1.750	.774
0	1.000	2.100	.650



Figure 1. — Sketch of the body showing dimensions and orifice locations.



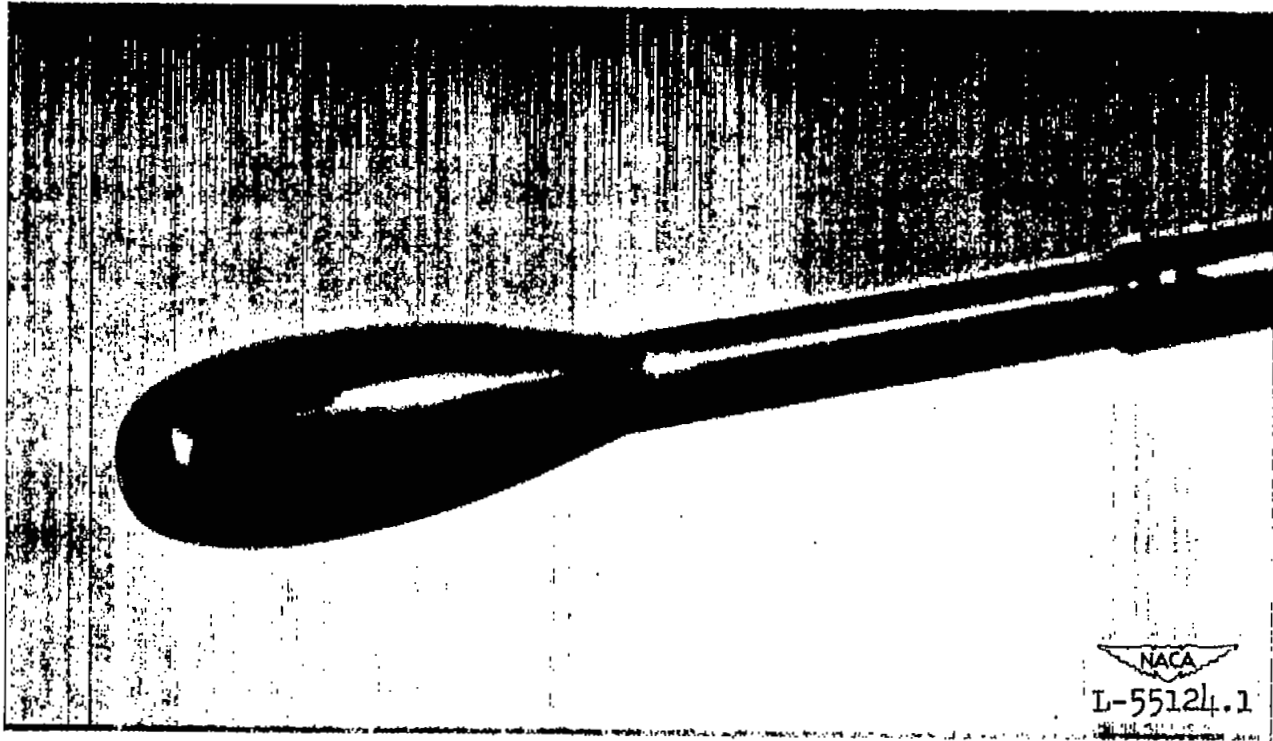
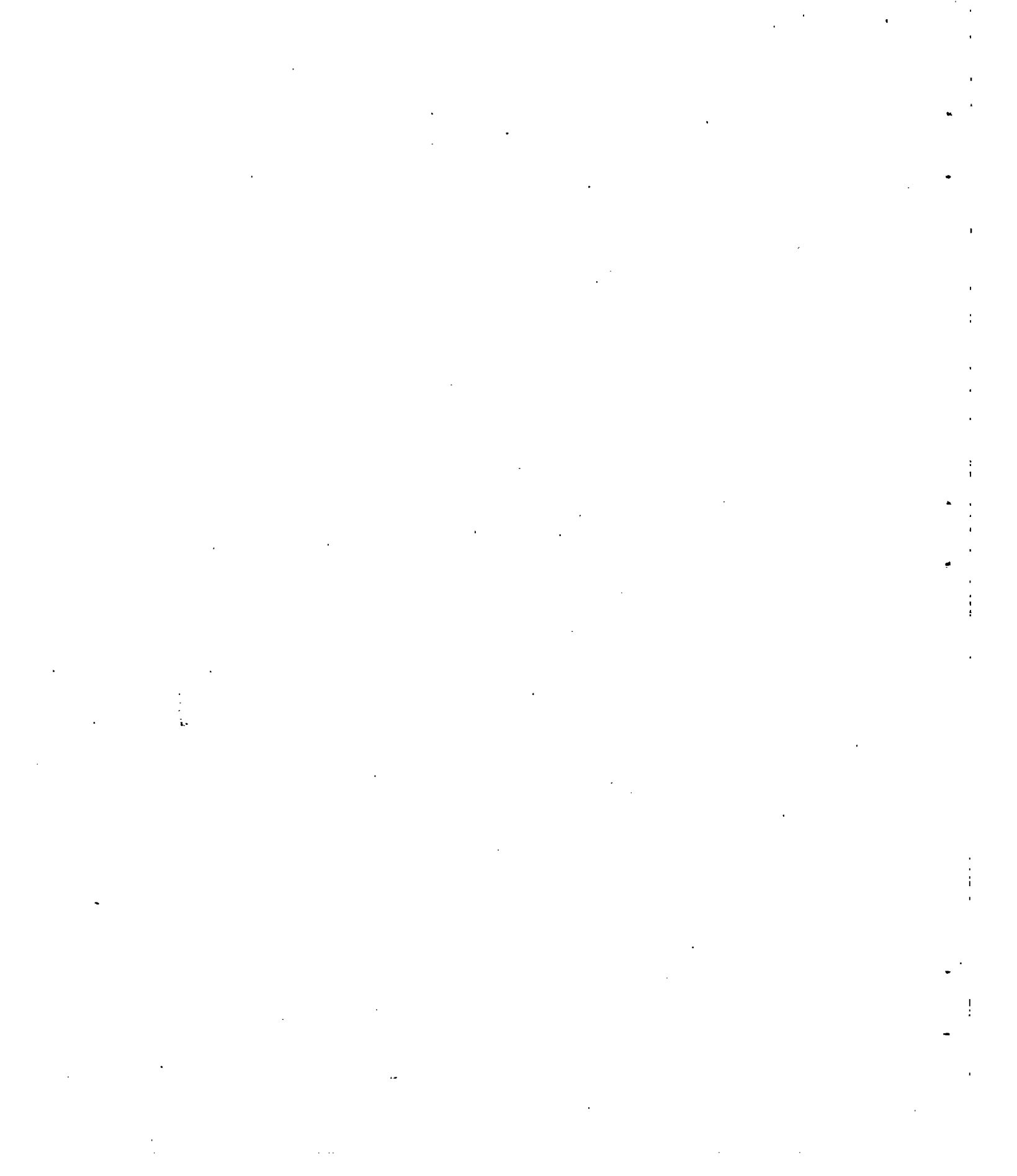


Figure 2.- Body of revolution with an NACA 1-50-100 nose inlet.



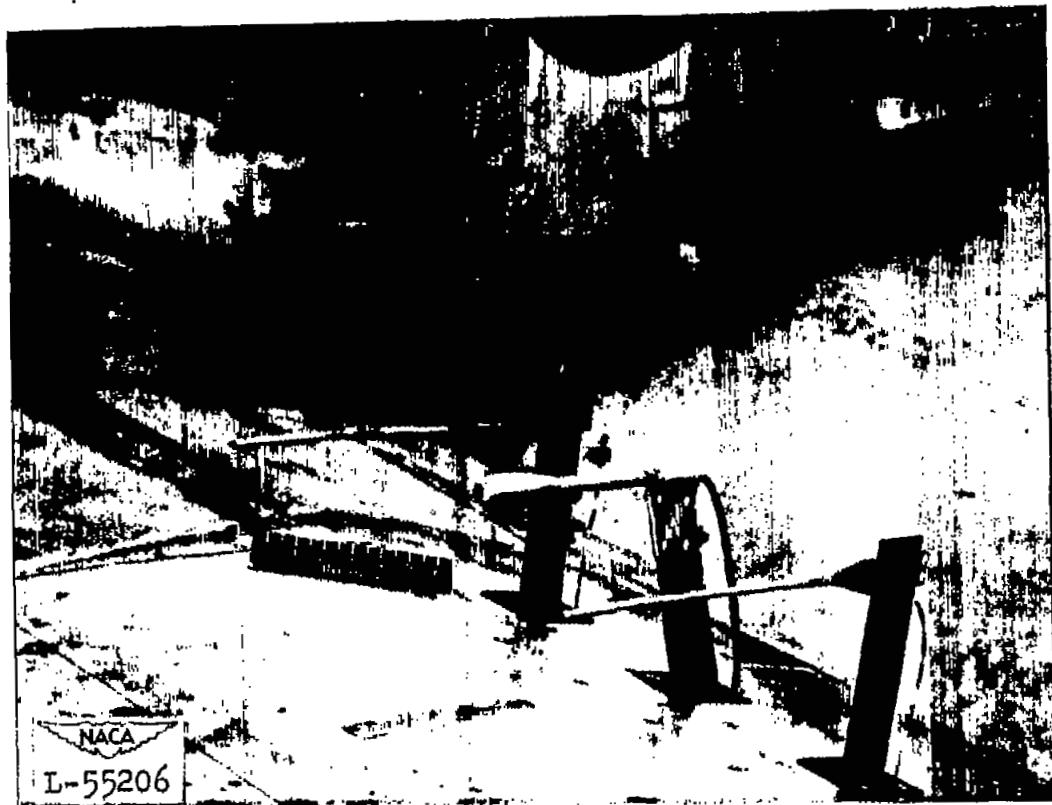
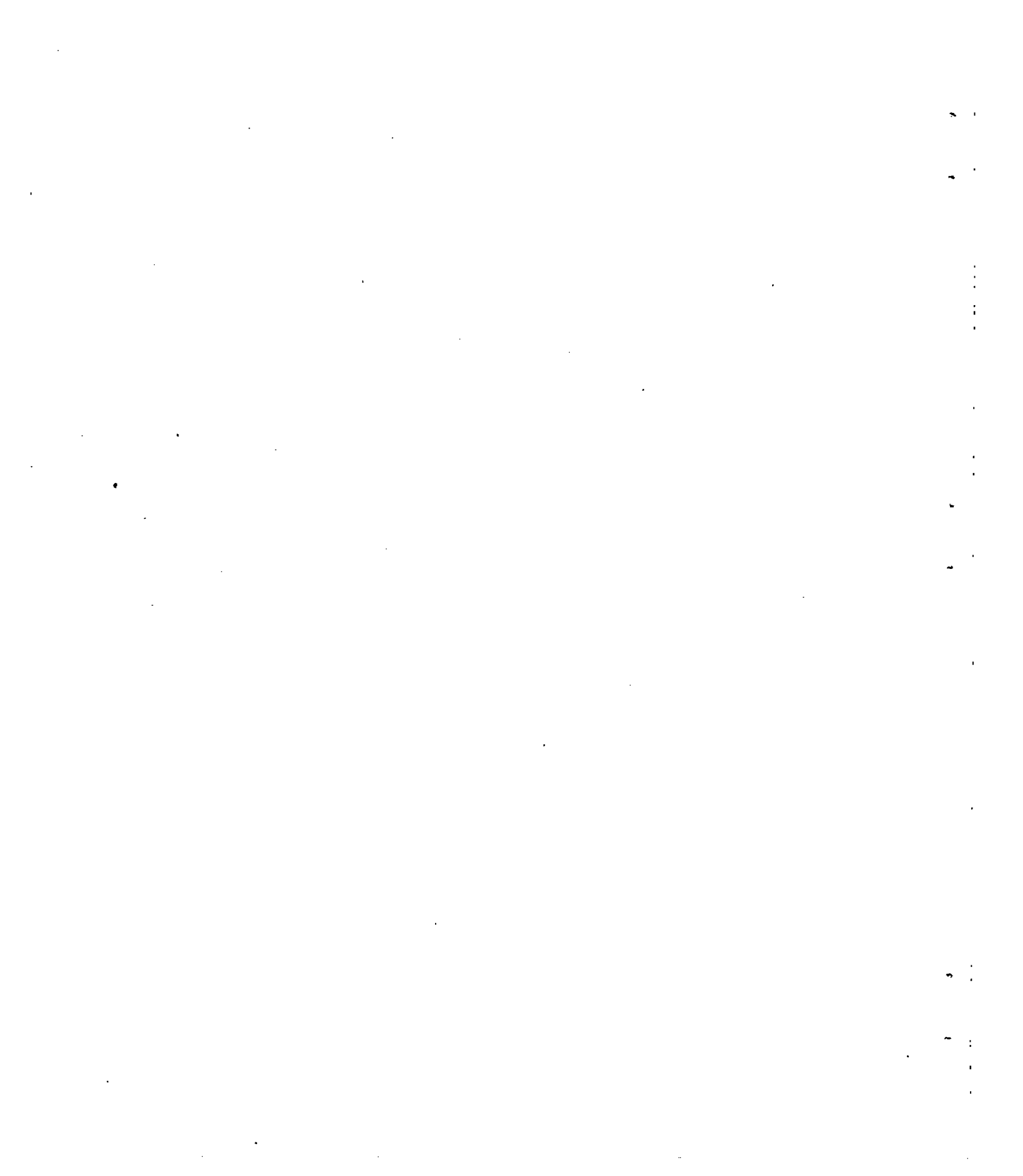


Figure 3.- Body-sting combination mounted on airplane wing with reference static-pressure tubes
8 inches on either side.



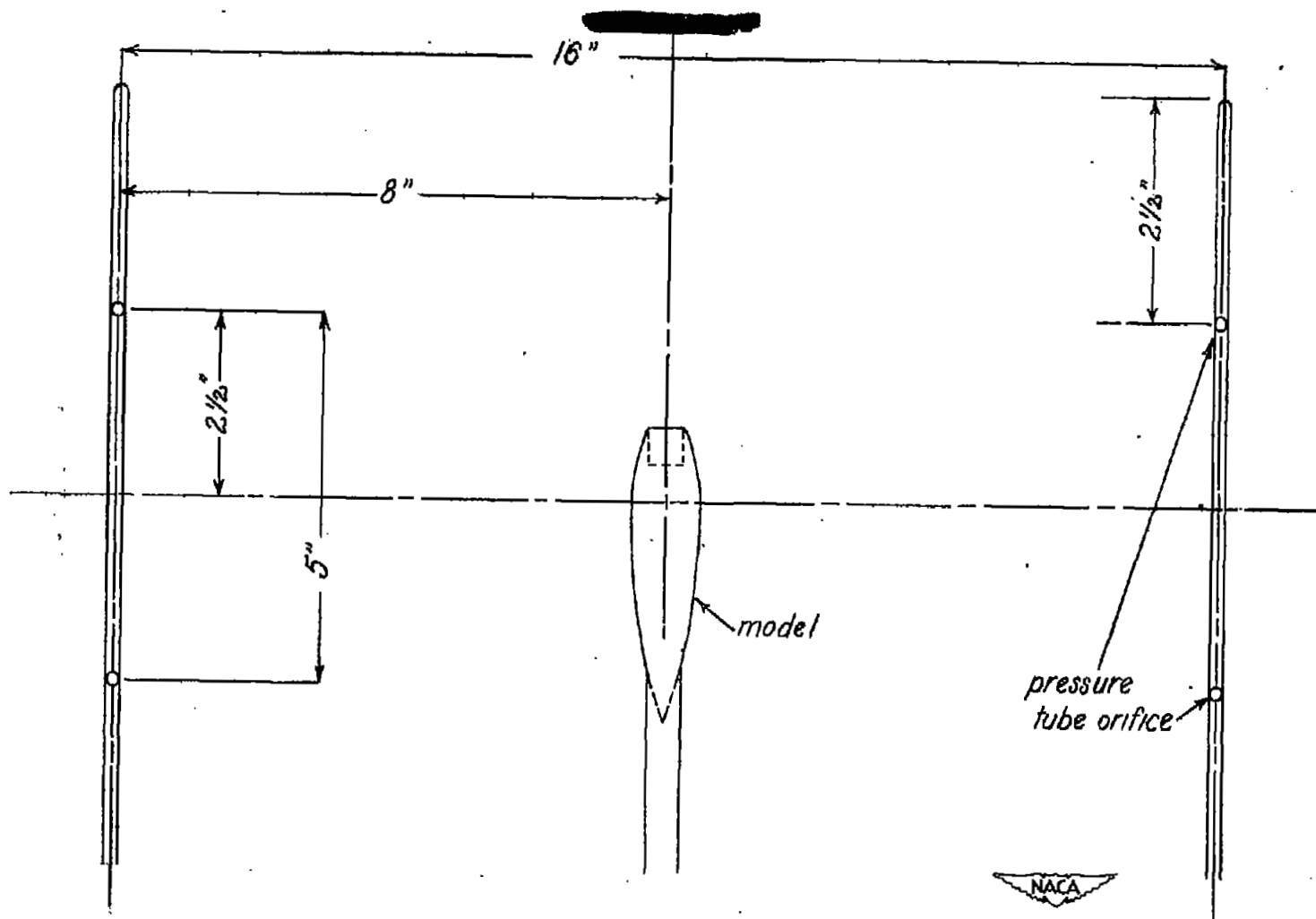


Figure 4.— Model and pressure tube locations
on test section.

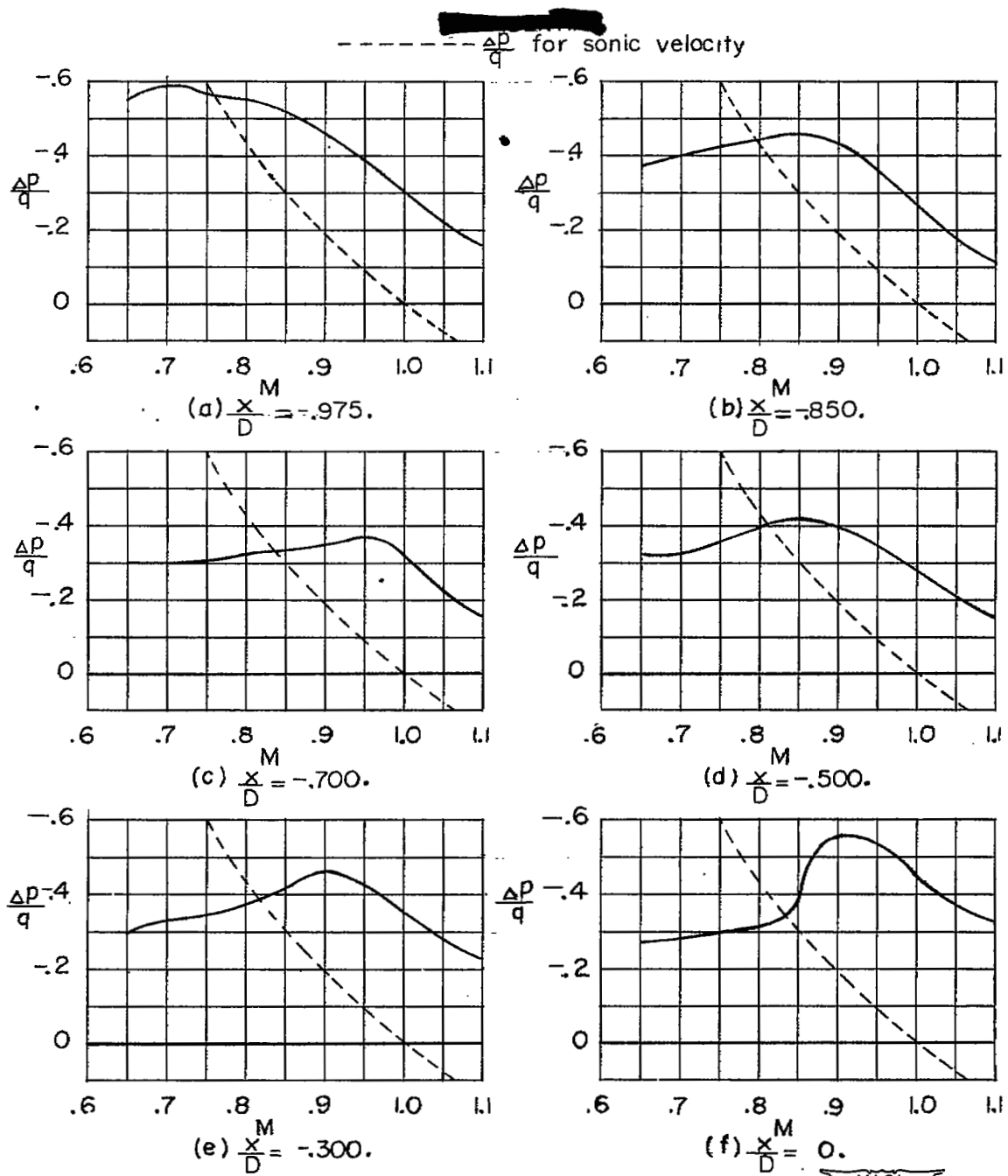


Figure 5. — Variation of $\frac{\Delta p}{q}$ with M at each orifice position.



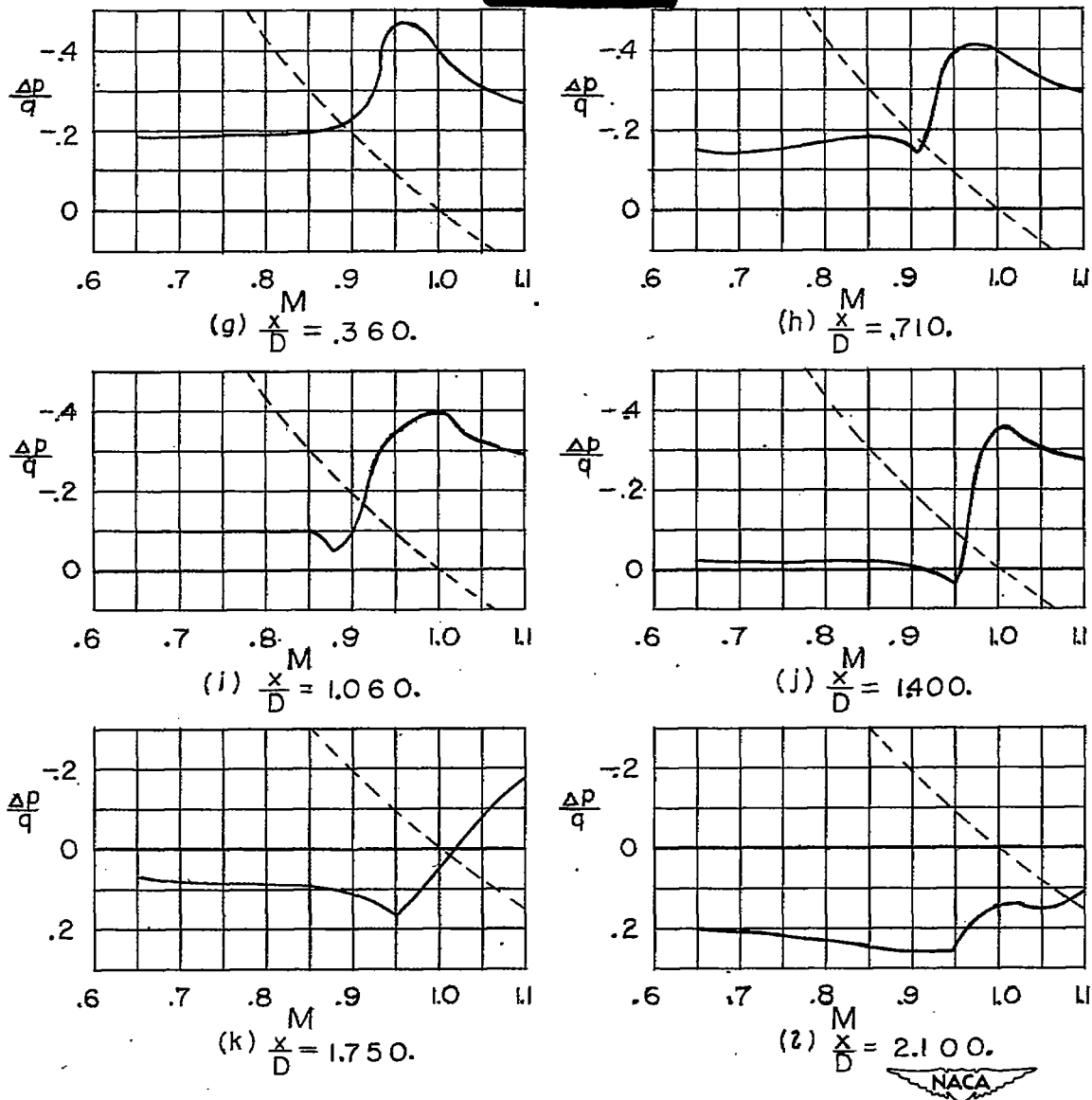


Figure 5. - Concluded.

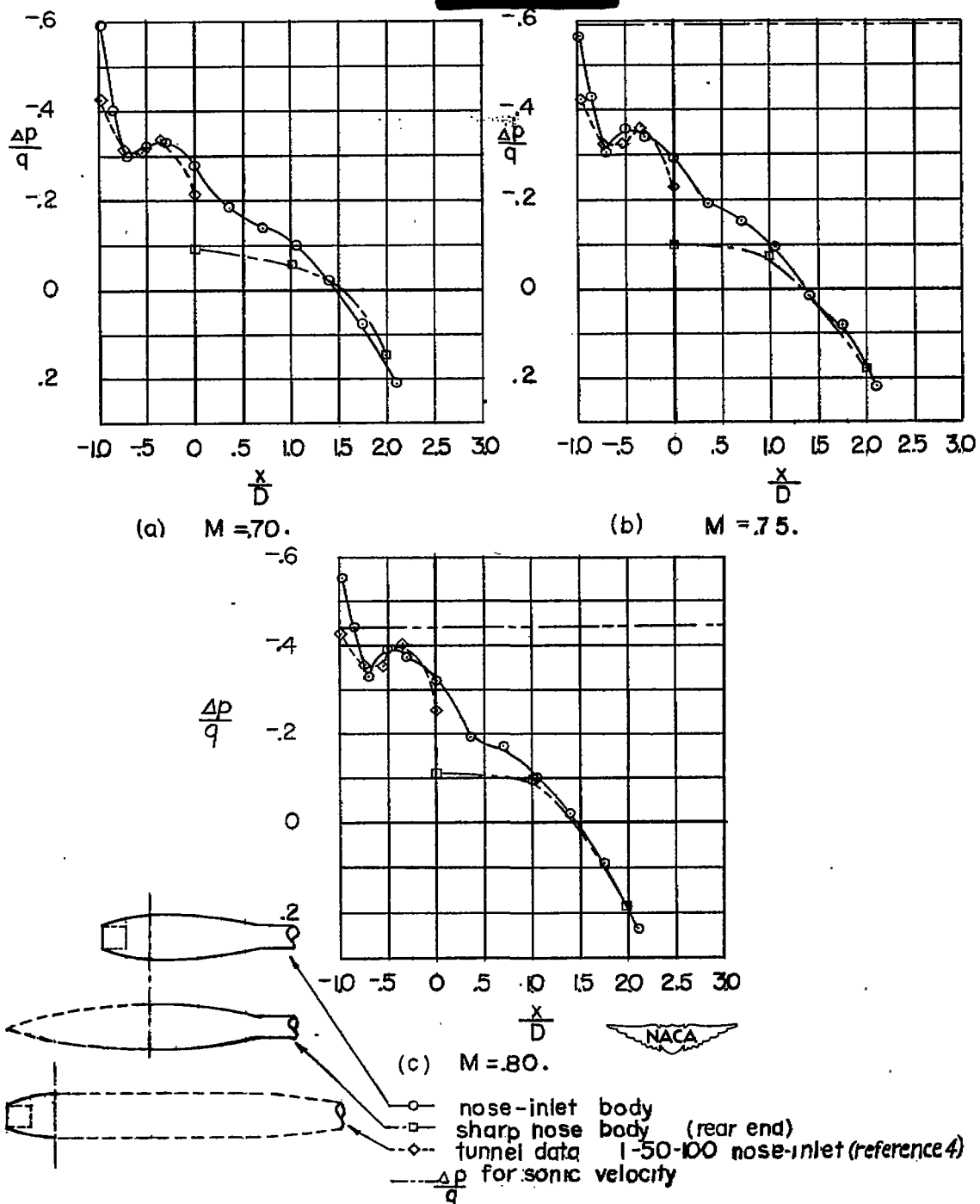


Figure 6.—Pressure distribution along axis
for various Mach numbers.

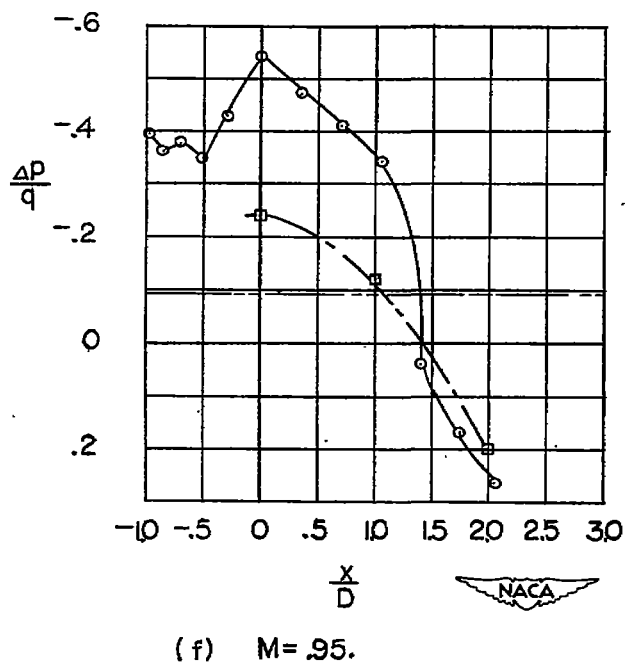
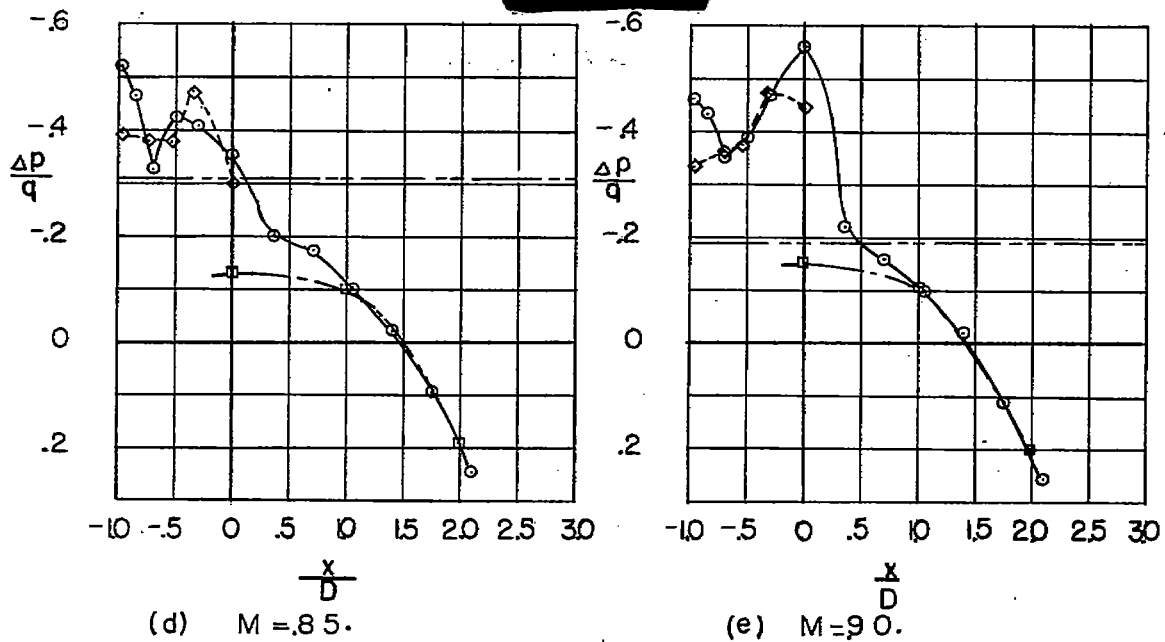


Figure 6 - Continued.

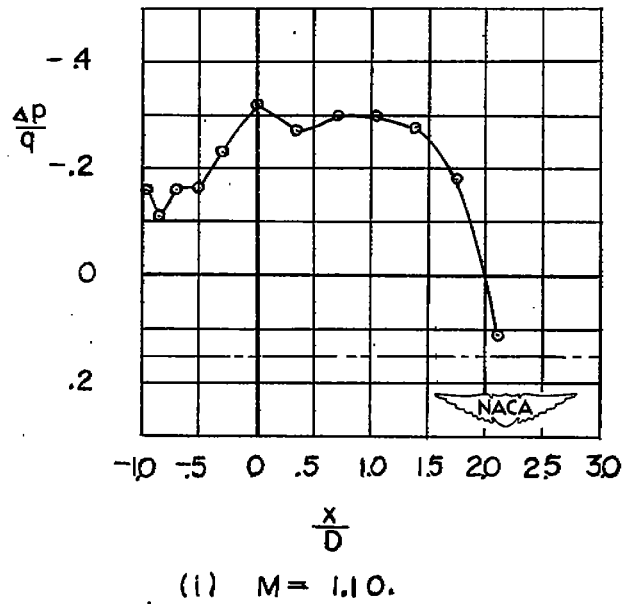
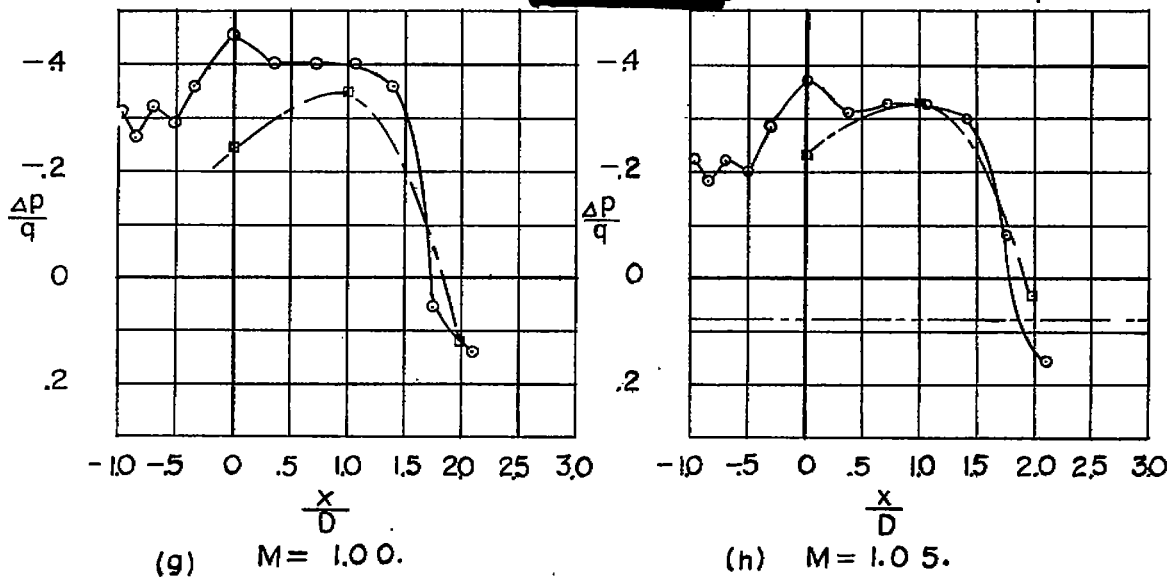


Figure 6.—Concluded.

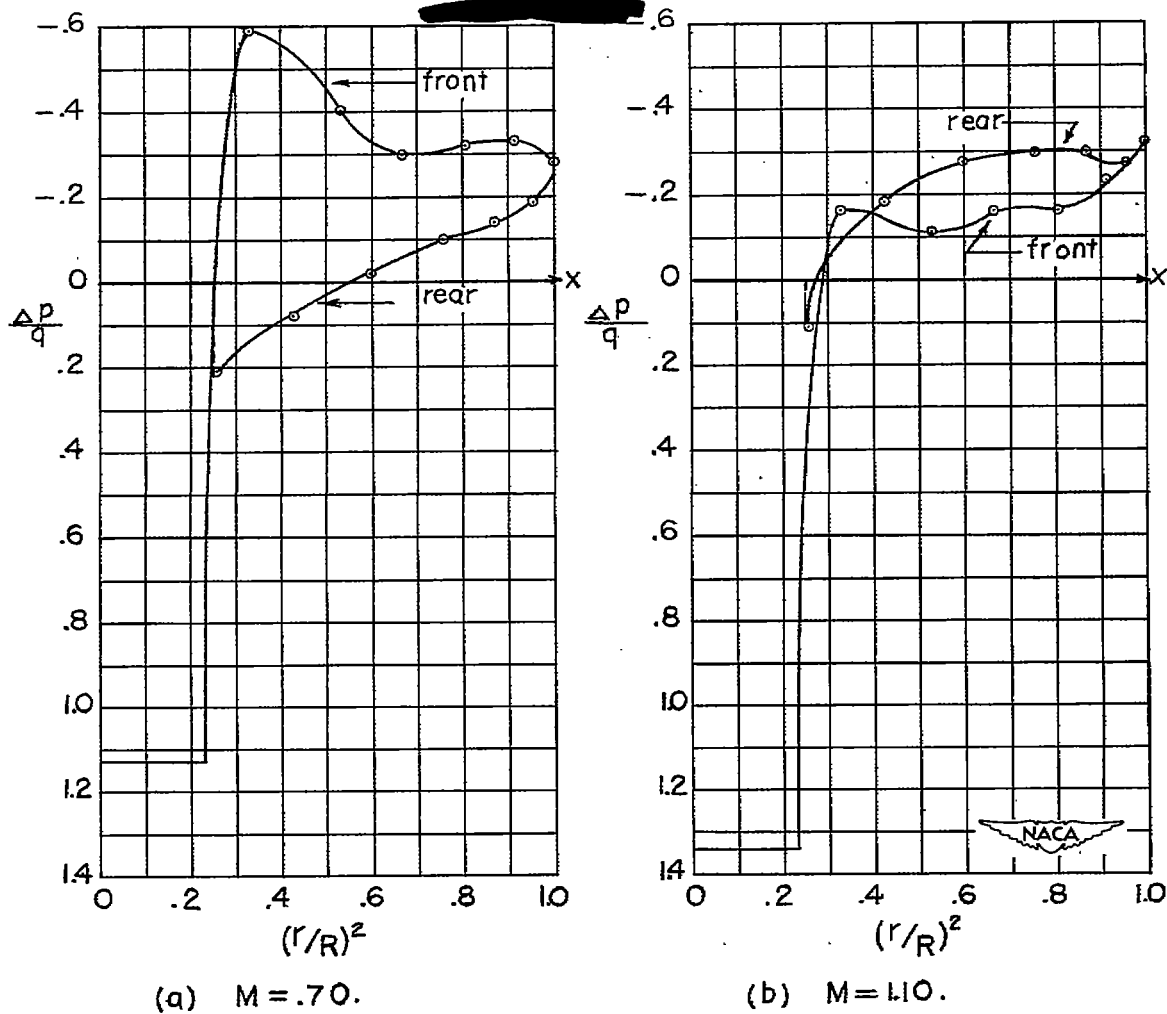


Figure 7.—Sample plots of $\frac{\Delta p}{q}$ against $(\frac{r}{R})^2$ used in determining the value of the pressure drag coefficient.

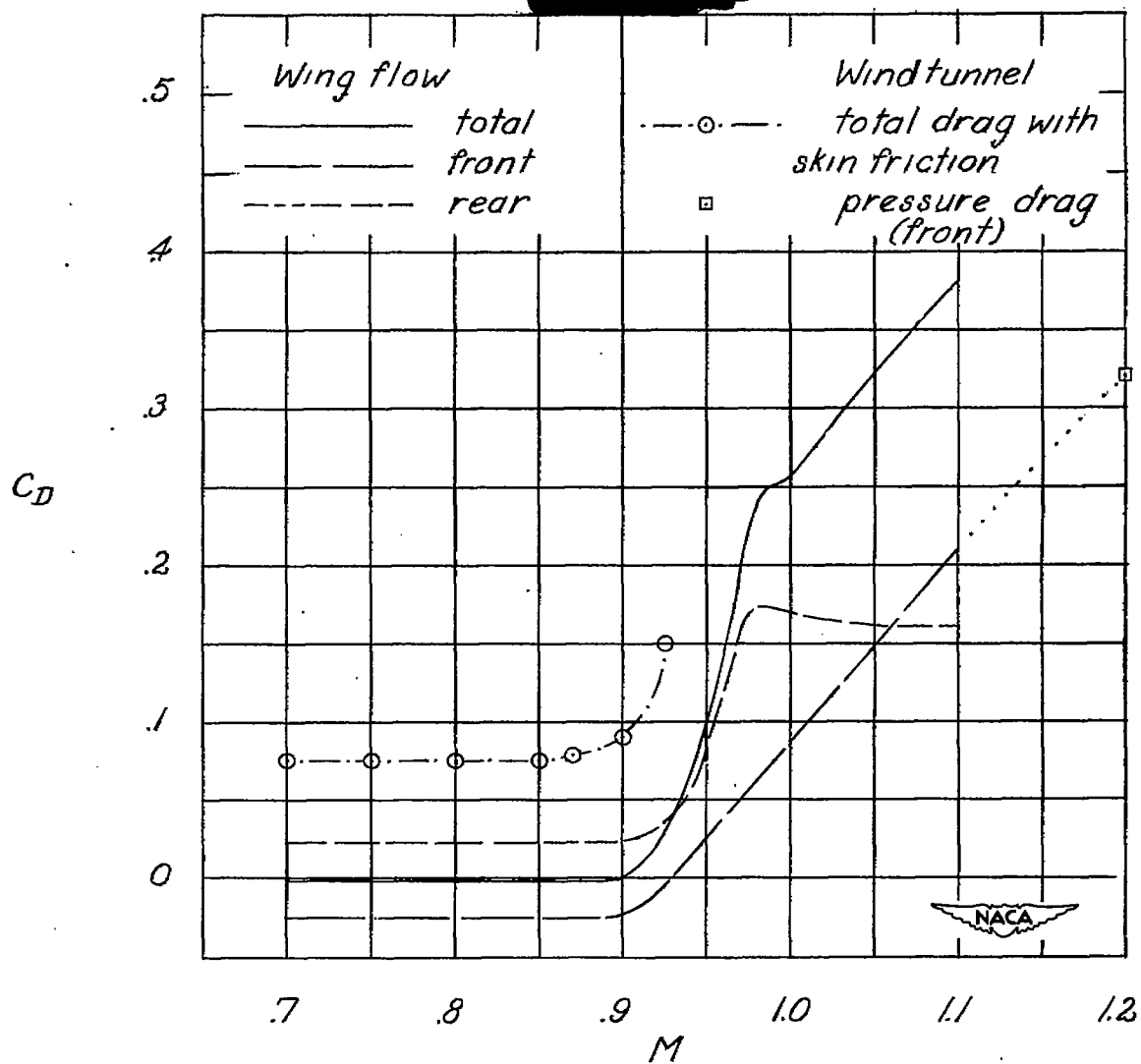


Figure 8. — Variation of C_D with
Mach number.

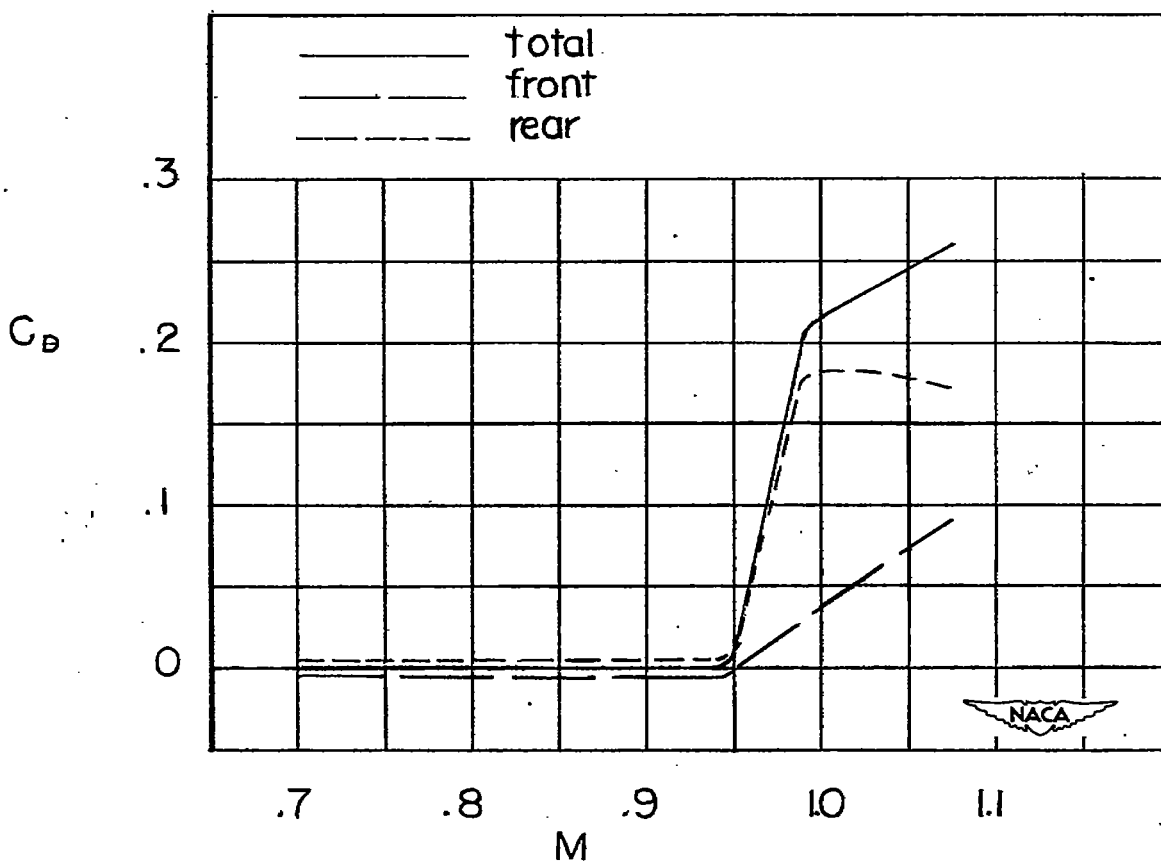


Figure 9. -Variation of C_D with Mach number of sharp-nose body in reference 1.

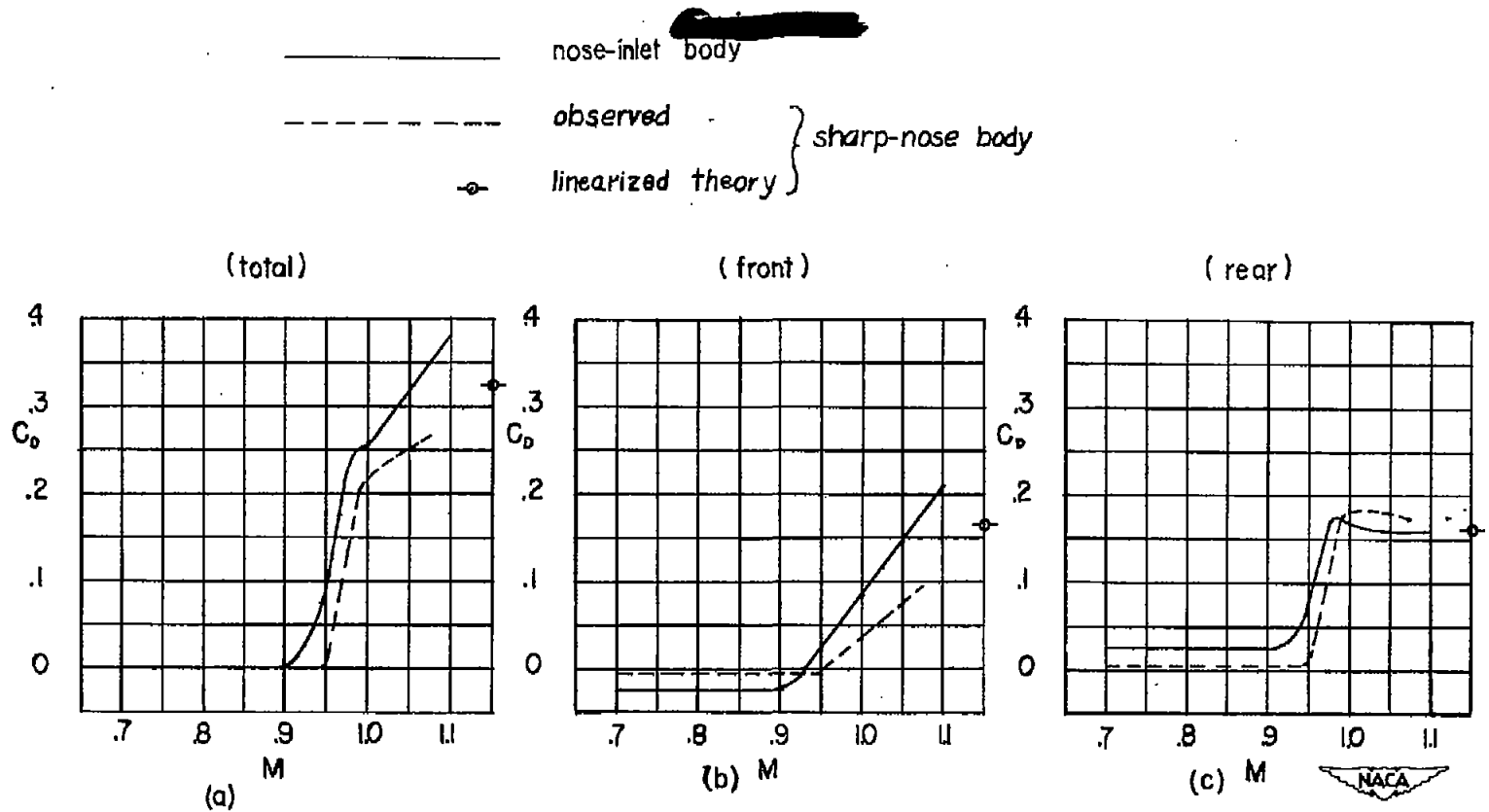


Figure 10.-Variation of C_D with Mach number of both nose-inlet and sharp-nose bodies

NASA Technical Library



3 1176 01436 7255

12/15